

PFC/JA-95-25

Disruptions and Halo Currents in Alcator C-Mod

R.S. Granetz, I.H. Hutchinson, J. Sorci,
J. Irby, B. LaBombard, D. Gwinn

July, 1995

Submitted to Nuclear Fusion.

This work was supported by the U. S. Department of Energy Contract No. DE-AC02-78ET51013. Reproduction, translation, publication, use and disposal, in whole or in part by or for the United States government is permitted.

Disruptions and Halo Currents in Alcator C-Mod

R.S. Granetz, I.H. Hutchinson, J. Sorci, J. Irby,
B. Labombard, D. Gwinn

MIT Plasma Fusion Center

Abstract

Disruptions in Alcator C-Mod can generate large eddy currents in the highly conducting vacuum vessel and internal structures, including a significant poloidal component due to halo currents. In order to better understand the stresses arising from the resulting $J \times B$ forces, Alcator C-Mod has been fitted with a comprehensive set of sensors to measure the spatial distribution and temporal behavior of the halo currents. It is found that they are toroidally asymmetric, with a typical peaking factor of 2. The asymmetric pattern usually rotates toroidally at a few kHz, thus ruling out first-wall non-uniformities as the cause of the asymmetry. Analysis of information compiled in the C-Mod disruption database indicates that the maximum halo current during a disruption scales roughly as either I_p^2/B_ϕ or I_p/q_{95} , but that there is a large amount of variation which is not yet understood.

I. Introduction

Disruptions are of great concern to tokamaks, primarily because of the potential for damaging the divertor, first wall, and/or other plasma facing components. Disruption damage can be manifested in several different ways, including melting and vaporization of large quantities of surface material due to direct thermal deposition, and structural failures caused by forces due to currents induced in conducting structures by fast transients^[1,2]. Alcator C-Mod, by virtue of its high magnetic field, high plasma current, compact size, and shaped plasmas^[3] is particularly well-suited for studying very fast disruption current quenches (instantaneous dI_p/dt up to 1.4 MA/ms). The vacuum vessel is a thick-walled (up to 5 cm) stainless steel structure with no insulating breaks, and therefore its one-turn resistance is only $40 \mu\Omega$ in the toroidal direction and $\sim 10 \mu\Omega$ in the poloidal direction^[4].

As a result, very large eddy currents, both toroidal and poloidal, can be induced in the vessel walls during disruptions. Induced toroidal currents, and the $J \times B$ forces they give rise to, can be reasonably well understood and modelled with axisymmetric plasma/circuit models, as used in codes such as TSC^[5]. However, induced *poloidal* currents are neither well understood, nor even sufficiently characterized experimentally, despite the fact that they can also give rise to forces on the vessel and internal hardware^[6]. In particular, questions about magnitude, scaling, toroidal asymmetry and peaking, radial distribution, temporal behavior, driving terms, current path, etc. need to be addressed before structural forces can be reasonably estimated. The desire to better understand these issues in Alcator C-Mod is the primary motivation for the work described in this paper. Since C-Mod is in some ways prototypical of future reactor designs, it is expected that these results will also be useful for specifying disruption-related engineering constraints.

II. Disruptions and VDE's in Alcator C-Mod

Disruption behavior in Alcator C-Mod is similar to that of other tokamaks running elongated plasmas^[7,8,9]. About 1/3 of all discharges end in a major disruption, although in certain restricted operational scenarios, the rate can be less than 5%. Disruptions due to excessive impurity radiation, excessive density (above the Greenwald limit^[10]), excessive plasma current ($q \leq 2$), and $n = 1$ locked modes have all been observed. Whatever the specific mechanism, the result is a sudden increase in energy transport throughout the entire plasma volume, leading to a very rapid loss of plasma temperature and dump of thermal energy. This phenomenon is commonly called the 'thermal quench' and an example as seen with the side-viewing x-ray array data is shown in figure 1a. In Alcator C-Mod, the energy loss time is typically 0.5 ms. Quite often, a series of minor disruptions (i.e. partial thermal losses) leads up to the final thermal quench. Much of this energy is radiated to the walls, but some fraction is conducted in the scrape-off layer to the separatrix strike points, possibly leading to high thermal power loads in the divertor. At the time of the thermal quench there occurs a momentary 10-15% increase ('spike') in the plasma current, as shown in figure 2, accompanied by a large negative spike in the loop voltage. Both of these classic disruption signatures are the result of a sudden flattening of the current profile^[11].

The fast drop in β_p and ℓ_i at the quench leads to a rapid inward shift of the magnetic axis. In vertically elongated plasmas, this new equilibrium also results in a significant and rapid increase in κ , as seen in the 2nd frame of figure 3, which shows a series of magnetic flux reconstructions at 1 ms intervals[†]. Depending upon the details of the vertical position feedback control, this rapid change in κ may cause the plasma to become vertically unstable, leading to the growth of the $n=0$ (i.e. axisymmetric) mode, and terminating in plasma contact with internal hardware at the top or bottom of the vacuum vessel. In Alcator C-Mod disruptions, virtually all ($> 99\%$) non-circular plasmas are lost vertically following the thermal quench. About 80% move towards the x-point. The timescale of this vertical drifting phase is characteristically several milliseconds, as seen in the final frames of figure 3, and the terminal plasma velocity is typically ~ 60 m/s. During this time, the plasma cross-sectional area is shrinking at about 30 to 80 m²/s, and the plasma current is decaying, albeit relatively slowly. Because of contact with the first wall (usually the inner and outer divertor hardware), the plasma equilibrium eventually switches from a diverted configuration to a limited one. At this time (typically 4-5 milliseconds after the thermal quench) the final stage of the disruption begins. As shown in figure 2, this consists of a rapid drop of the remaining plasma current, accompanied by appreciable current flowing poloidally in the vessel structure. These poloidal currents are known as ‘halo’ currents^[12], and will be discussed in detail in the next section. This final phase is commonly called the ‘current quench’, and in Alcator C-Mod its duration is usually 1-2 ms. Much of the stored magnetic field energy of the plasma current is transferred to nearby conducting structures via induced eddy currents, but some can also be converted directly into particle kinetic energy during the current quench, and eventually is deposited on plasma-facing components.

The preceding disruption scenario (thermal quench *followed* by vertical drift *followed* by current quench) covers many of the disruptions on Alcator C-Mod. However, there is a

[†]These flux reconstructions are calculated by using a set of axisymmetric filaments at fixed positions inside the vessel to model the plasma, and additional filaments to account for external PF coils and axisymmetric eddy currents in the conducting structure. The amplitudes of the filament currents at any given time are determined by a least-squares fit to the fluxes and fields measured by the magnetics diagnostics. The time resolution is limited only by the digitization rate.

significant proportion of disruptions which are actually *initiated* by a loss of vertical position control, rather than by a thermal quench. This can be due to running excessively elongated plasmas, or to occasional problems with the feedback stabilization system, or even to intentionally disabling the vertical position control. The end result is that the plasma hits the top or bottom of the vessel and *then* disrupts, as shown by the side-viewing x-ray array in figure 1b. These types of disruptions are often called vertical displacement events, or VDE's^[13]. In Alcator C-Mod, the characteristics of the current quench and halo currents in VDE disruptions are similar to those of non-VDE disruptions, as shown in figure 4. The primary difference is that VDE's do not begin with a thermal quench. Therefore in VDE disruptions, the plasma hits the vessel top or bottom with all of its stored kinetic energy as well as its magnetic energy. There is usually still an identifiable thermal quench at that time, followed immediately by the current quench. Since the electromagnetic effects of VDE's and thermal quench disruptions in Alcator C-Mod are similar, the results discussed in the remainder of this paper apply to both classes of disruptions.

III. Halo Current Diagnostics on Alcator C-Mod

It is now known that during disruptions, significant current flows on open field lines in the scrape-off plasma outside of the last closed flux surface^[14,15]. This 'halo' current flows into the vessel wall (or other conducting plasma-facing components) where one end of the open field lines contact, and flows out at the other end, thus forming a closed circuit which has a *poloidal* component. Since there is no appreciable plasma pressure on open field lines, the halo current presumably must flow in a nearly force-free configuration through the plasma exterior, i.e. along helical field lines. However, in the surrounding conducting structures there is no force-free restriction, and purely poloidal current is possible. (The exact current path in the structure depends upon its impedance and the direction of any induced electric fields). In any case, the halo current has a finite poloidal component, and coupled with a tokamak's strong toroidal field, large forces can be exerted on conducting structures. Note that this is *in addition* to forces arising from induced toroidal eddy currents. Furthermore, stresses on the vessel and conducting structures may be exacerbated even further if the halo currents are appreciably non-axisymmetric, i.e. exhibiting a locally peaked distribution toroidally.

In order to address these issues, Alcator C-Mod has been fitted with an extensive set of sensors for measuring the magnitude and spatial variation of poloidal halo currents during disruptions. These consist primarily of full Rogowski coils (which measure I through the closed coil loop), segmented Rogowski coils (which measure $\int B_\phi d\ell$ over 1/10 of the toroidal circumference), and current shunts (which measure a voltage drop across a known resistance).

Because of the $1/R$ dependence of the toroidal field, the highest $\mathbf{J}_{\text{pol}} \times \mathbf{B}_\phi$ forces will be on the inboard wall of the vacuum vessel, so it is important to know the halo current flowing vertically in that region. Two Rogowski coils completely encircle the inner wall, one at the top of the machine, the other at the bottom, as shown in figure 5a. They occupy a small tunnel at the corner of two intersecting plates of protection tiles, and are therefore well protected from exposure to the plasma. Each winding measures the total current flowing vertically in the wall at the top and bottom, respectively. The TF magnet current (27 MA-turns at 8 T) also passes through these Rogowskis, and dominates the signal. During the initial operation of these full Rogowski coils, this TF pickup was quite useful for verifying coil integrity and for in-situ calibration. Thereafter, the slowly-varying TF contribution was filtered out by simple AC-coupling of the signals.

Toroidal variation of halo currents is measured independently by two different sets of sensors in two different locations, namely segmented Rogowski coils and current shunts. As shown in figure 5b, the set of segmented Rogowski coils is conceptually a full Rogowski divided up into ten segments, and it is located immediately adjacent to the previously described full Rogowski on the bottom of the machine. The choice of 10 segments was dictated by the structure of the vacuum vessel, which has a ten-fold symmetry (i.e. 10 sets of ports, 10 divertor modules, etcetera). The top of the machine is not yet instrumented with segmented Rogowski coils.

There is also a set of 10 current shunts, one for each of the outboard divertor modules. Were it not for these shunts, the divertor modules would be electrically isolated from the vacuum vessel, but the shunts provide a conducting path through a mechanical attachment to the vessel. Each shunt has a resistance of $0.4 \text{ m}\Omega$, and the halo current flowing from the vessel through the divertor module into the plasma boundary is determined by measuring the voltage drop across the shunt. Note that the shunts and the segmented Rogowski

coils enable independent measurements of the toroidal distribution of halo currents at *two different poloidal locations* — bottom inboard and bottom outboard.

Finally, an additional set of four segmented Rogowskis, each also $\frac{1}{10}$ of a toroidal turn, has been installed along part of the inboard vessel wall at a single toroidal location, in order to determine the thickness and distribution of the current flowing in the halo layer as it enters the vessel wall. As shown in figure 5c, the sensors are installed at four different vertical positions spaced 10 cm apart, from the inner divertor region up to the midplane.

IV. Halo currents

Extensive measurements of halo current magnitudes, directions, temporal behavior, and spatial distribution have been, and are continuing to be studied during Alcator C-Mod disruptions using the instrumentation described in the preceding section.

The halo diagnostic signals are digitized at rates up to 1 MHz for each disruption. A subset of this data, such as peak halo current, peak dI_p/dt , disruption direction, etc. is also compiled in a disruption database, which is useful for discerning general trends in the data. In this section, the behavior of the total poloidal halo current, as measured by the full Rogowski coils in figure 5a, will be described. Following sections will detail the toroidal and poloidal distribution of halo currents.

Figure 2 shows the temporal behavior of the total poloidal halo current at the top and bottom of the inboard wall of the vacuum vessel during a typical disruption (i.e. a thermal quench followed by downward motion). A significant amount of halo current flows in the bottom of the machine, while very little is seen at the top. In the $\sim 20\%$ of cases in which the disrupting plasma moves upwards, this behavior is reversed; significant halo current flows only at the top of the machine. Unlike the magnitude, the *direction* of the poloidal current flowing in the inboard wall of the vacuum vessel is independent of the direction of plasma vertical motion. For the disruption exhibited in figure 2, for which B_ϕ and I_p are in a clockwise direction when viewing down on the torus from above, the halo currents in the inboard wall flow downward, as indicated by the arrows in figure 3. When the toroidal field and plasma current are reversed, the poloidal halo current reverses direction as well. (C-Mod is always operated with co-parallel B_ϕ and I_p .) Thus, in all cases the total poloidal halo current flows in the direction which generates a $\mathbf{J}_{\text{pol}} \times \mathbf{B}_\phi$ force

tending to oppose both the vertical motion of the plasma, and the reduction in toroidal flux due to the shrinking cross-section. Of course, the halo current flowing around the plasma exterior must presumably be following helical field lines in order to be force free, and therefore has a large toroidal component (not shown in figure 3).

The temporal behavior of the total halo current closely resembles dI_p/dt , which is also shown in figure 2. In particular, the halo current peaks at about the same time that the maximum in dI_p/dt occurs — typically several milliseconds after the thermal quench. In fact, for virtually all vertically-moving disruptions (both VDE's and non-VDE's), the bulk of the current loss, the bulk of the halo current, and contact with structure at the top or bottom of the machine all occur simultaneously. In marked contrast, the plasma cross-sectional area starts decreasing as soon as the plasma begins moving away from the midplane, as shown in figure 2. This suggests that the driving voltage for halo currents may be due to the toroidal electric field generated by dI_p/dt rather than any poloidal electric field generated by reduction of magnetic flux within the plasma cross-section. (Presumably both toroidal and poloidal electric fields could drive halo currents, since they should flow helically around the plasma.)

As mentioned previously, data on halo currents, as well as other disruption phenomena, are compiled into a database, which is useful for determining trends in the data. In figure 6, the peak upper and lower halo currents, as measured by the full halo Rogowski coils, are plotted vs. I_p for all downward-going disruptions with $|B_\phi| = 5.3$ T. (The plasma current plotted here is the value just prior to the disruption.) Clearly, the bulk of the halo current flows in the vicinity of the vacuum vessel toward which the plasma moves. At this toroidal field (which constitutes the bulk of plasma operation to date), the peak halo current increases roughly quadratically with plasma current, although there is a large amount of scatter in the data. Operations over a large range in toroidal field ($1.5 \leq |B_\phi| \leq 8.2$ T) indicate an inverse scaling with B_ϕ , leading to either an I_p^2/B_ϕ or an I_p/q_{95} scaling, as shown in figure 7.

A scaling law for peak halo current may be useful for extrapolating to the higher I_p and B_ϕ operational parameters that are planned for Alcator C-Mod. However, there is a considerable amount of scatter in the data, so it is also important to have an estimate of the variation, and of the 'worst-case' value of peak halo current as well. Figure 8 shows the probability distribution of the ratio of peak halo current to I_p for disruptions

with $B_\phi = 5.35$ T and $I_p = 0.8$ MA. For these parameters, the mean ratio is 15%, but the distribution ranges about ± 5 percentage points about the mean, or about $\pm 1/3$. We currently have no explanation for this variation. In addition, there are a handful of cases above 30%, with the worst having a peak halo current of 50% of I_p . We know that the most extreme outliers occurred when the horizontal field power supplies saturated while trying to run unusual plasma shapes, so it is possible to avoid these cases.

The disruption database also contains information on the peak current quench rate for each disruption. The peak current quench rate is defined as the maximum instantaneous amplitude of dI_p/dt during a disruption. The derivative is not smoothed, i.e. it is calculated by the simple two-point difference method. On Alcator C-Mod, the peak quench rate scales roughly linearly with I_p , which indicates that the timescale for the bulk of the current loss is ~ 1 – 2 ms, independent of plasma current, as shown in figure 9. This is consistent with the signals shown in figures 2 and 4. As with the peak halo currents, there is a considerable amount of scatter in the data, particularly for upward-going disruptions. Despite the scatter, it is apparent from figure 9 that the fastest current quenches occur in upward or centered disruptions. Note that there is no upper divertor in C-Mod, and thus there is less conducting structure at the top of the vacuum chamber compared to the bottom.

V. Toroidal distribution of halo currents

Mechanical stresses arising from $\mathbf{I}_{\text{halo}} \times \mathbf{B}_\phi$ in the vacuum vessel, first wall, and other conducting structures can be greatly exacerbated if the halo currents are not uniformly distributed toroidally. Measurements of the toroidal distribution of halo current using the array of ten divertor shunts is shown in figure 10 for three different times during a disruption. The time slices are separated by about $100 \mu\text{s}$. In each time slice, the toroidal distribution is clearly not uniform, with a peak-to-average value of ~ 2 , and a structure which can be roughly described as a combination of an $n = 0$ component and an $n = 1$ component of comparable magnitudes. (Fourier analysis usually shows a small $n = 2$ component as well.) The degree of toroidal asymmetry changes from shot to shot, but this example is typical. Furthermore, from the different time slices it is apparent that the $n = 1$ structure is rotating at a few kHz, in the opposite direction of I_p and B_ϕ . This

rules out the possibility that the toroidal asymmetry in the halo current is due to first-wall non-uniformities or B -field misalignment. When I_p and B_ϕ are reversed, the halo rotation also reverses. In figure 11, data from the toroidal array of ten Rogowski segments is shown for the same shot. Because these sensors actually measure $\int B_\phi d\ell$ over one-tenth of the toroidal circumference, and since the halo currents are not toroidally symmetric, some modeling of the current flow is needed to independently obtain the magnitudes of the halo currents, but these are only weakly dependent on the model. The total current measured by summing up the toroidal array of halo Rogowski segments (with appropriate compensation for one segment which is not functional) is in excellent agreement with the full Rogowski measurement. The rotation frequency and behavior also changes from shot-to-shot, but this example is typical. In some cases the rotation slows down and even stops; in others the toroidal structure doesn't rotate at all. The rotation reverses direction when I_p and B_ϕ are reversed. So far, we have not discerned any correlation between the toroidal asymmetry and/or rotation of halo currents with global parameters of the disruption (i.e. dI_p/dt , q_ψ , type of disruption, etc).

Comparison of the toroidal distribution of halo currents measured by the segmented Rogowskis and by the divertor shunts show identical structure *and* identical phase with respect to toroidal angle (within the measurement resolution of $\frac{1}{10}$ of 360°), as shown in figure 12. This implies that within the stainless steel wall of the vacuum vessel, the halo current flows poloidally, with little or no toroidal component. This is not necessarily surprising, since the path of least resistance is poloidal, and the current flow does not have to be force-free. However, to complete the circuit, the halo current must leave the outer divertor at one end of the open field lines, flow across the top of the plasma in a presumably force-free, and thus *helical* direction, and re-enter the wall at the inboard end of the open field lines. The fact that our measurements show that the inboard and outboard halo currents have identical structure and phase implies that the helical flow must make an integral number of toroidal transits in going from the outboard to inboard contact points. Thus there may be a resonance in field line helicity involved in the flow of halo currents, and perhaps in the current quench itself. We are currently studying this interesting implication in greater detail.

VI. Poloidal distribution of halo currents

In addition to the measurements of the toroidal distribution of halo currents, there are also data on the vertical distribution, as measured by the set of segmented Rogowski coils described previously in section III and shown in figure 5c. Figure 13 shows the vertical array data for a typical downward disruption. Only the lowest-most sensor registers significant halo current. Halo current flows into the inboard wall only in the vicinity of the inboard divertor hardware, which indicates that the thickness of the halo current layer is rather small. The lack of appreciable signal on the next higher sensor places an upper limit on the halo layer thickness which corresponds to ~ 3 cm when mapped back to the plasma midplane. This example is representative of all downward-going disruptions. Curiously, the halo current seen in the lowest wall sensor always peaks noticeably after the halo current measured at the bottom of the vessel, possibly suggesting that the halo layer spreads upward at the very end of a downward-going disruption.

For the few disruptions which stay near the midplane, the halo diagnostics at the bottom and top of the vessel see no halo currents. However, the midplane sensor on the inboard wall does detect significant halo current, as shown in figures 14 and 15. The magnitude is comparable to that seen for vertical disruptions with similar plasma current and field. The next lower sensor in the inboard wall detects nothing, which is another indication that the halo current layer is thin. Although the number of vertically stable disruptions is very small, halo current is always seen on the midplane sensor in these cases. Therefore it is reasonable to conclude that *vertical motion by itself does not directly generate halo currents*. The axisymmetry of halo currents at the midplane is not measured.

VII. Summary

Due to its compact size, high B -field, high current density, and highly conducting vacuum vessel, disruptions in Alcator C-Mod result in substantial eddy currents and $\mathbf{J} \times \mathbf{B}$ forces on tokamak structures. Studies using a comprehensive set of diagnostics on C-Mod show that large halo currents are generated only during the current quench portion of disruptions, with a temporal evolution that closely resembles dI_p/dt , suggesting that halo currents are primarily driven by induced toroidal rather than poloidal electric fields.

Significant halo currents are observed only in the region of the vessel toward which the disrupting plasma moves. The halo currents have a large toroidal asymmetry, with a typical peak-to-average ratio of 2, and a predominantly $n = 1$ structure which usually rotates toroidally. They flow in a relatively thin layer (~ 3 cm) outside the last closed flux surface. Halo currents exist even in disruptions that remain positioned on the midplane. Analysis of our disruption database indicates that the maximum halo current during a disruption scales like I_p^2/B_ϕ or I_p/q_{95} , but that there is a large amount of variation, which for the most part is not understood. Data from the halo diagnostics are currently being used to refine engineering calculations of the stresses and deformations of the C-Mod vacuum vessel and internal components.

Acknowledgements

The authors wish to acknowledge the considerable efforts of the entire Alcator team for the successful operation of the C-Mod tokamak, and to Steve Wolfe for initially setting up the disruption database.

References

- [1] NOLL, P., AIGLE, R., BROWNE, M.L., *et al*, in Fusion Engineering (Proc. 11th Symp. Austin, TX, 1985), Vol. 1, IEEE, New York (1985) 33.
- [2] KUGEL, H.W., ASAKURA, N., BELL, R., *et al*, in Controlled Fusion and Plasma Physics (Proc. 16th Eur. Conf., Venice, 1989), Vol. 13B, Part I. European Physical Society (1989) 199.
- [3] HUTCHINSON, I.H., *et al*, Phys. Plasmas 1 (1994) 1511.
- [4] TINIOS, G. HORNE, S.F., HUTCHINSON, I.H., WOLFE, S.M., "Model Reduction for Axisymmetric Tokamak Control", MIT Report PFC/JA-92-35 (1992).
- [5] JARDIN, S.C., POMPHREY, N., DELUCIA, J., J. Comput. Phys. 66 (1986) 481.
- [6] PICK, M.A., NOLL, P., BARABASCHI, P., MARCUS, F.B., ROSSI, L., "Evidence of Halo Currents in JET", in Proceedings of the 14th Symposium on Fusion Engineering, San Diego (1991) 87.
- [7] YOSHINO, R., NEYATANI, Y., HOSOGANE, N., *et al*, Nucl. Fusion 33 (1993) 1599.
- [8] TAYLOR, P.L., KELLMAN, A.G., EVANS, T.E., *et al*, "Experimental Disruption Studies in DIII-D", Bull. Am. Phys. Soc. 39 (1994) 1650.
- [9] WESSON, J.A., *et al*, Nucl. Fusion 29 (1989) 641.
- [10] GREENWALD, M., TERRY, J., WOLFE, S., EJIMA, S., BELL, M., KAYE, S., NEILSEN, G.H., Nucl. Fusion 28 (1988) 2199.
- [11] KADOMTSEV, B.B., in Plasma Physics and Controlled Nuclear Fusion Research 1976 (Proc. 6th Int. Conf., Berchtesgaden, 1976), Vol. 1, IAEA, Vienna (1977) 555.
- [12] STRAIT, E.J., LAO, L.L., LUXON, J.L., REIS, E.E, Nucl. Fusion 31 (1991) 527.
- [13] THOMAS, P.R., WESSON, J.A., ALLADIO, F., *et al*, in Plasma Physics and Controlled Nuclear Fusion Research 1984 (Proc. 10th Int. Conf., London, 1984), Vol. 1, IAEA, Vienna (1985) 353.
- [14] GRUBER, O., LACKNER, K., PAUTASSO, G., SEIDEL, U., STREIBL, B., Plasma Phys. Control. Fusion 35 (1993) B191.
- [15] JENSEN, T.H., CHU, M.S., Phys. Fluids B 1 (1989) 1545.

List of Figure Captions

- Figure 1a — Typical thermal quench disruption as seen with the horizontally-viewing x-ray array. A series of minor disruptions are followed by a sudden major disruption at $t = 0.869$ s. Subsequently, vertical position control is lost and the plasma moves downward toward the x-point.
- 1b — Typical VDE disruption as seen with the horizontally-viewing x-ray array. Note that the plasma retains its thermal energy until contacting the divertor structures at the bottom of the vessel.
- Figure 2 — Evolution of the plasma current, halo currents, position, and cross-sectional area during the thermal quench disruption shown in Fig. 1a.
- Figure 3 — Magnetic flux reconstructions at 1 ms intervals for the disruption in figure 1a. The arrows show *the poloidal projection* of halo current flow, which exists primarily during the last two frames. In order to be force-free, the portion of the halo circuit in the plasma scrape-off must actually follow a helical path.
- Figure 4 — Evolution of the plasma current, halo currents, position, and cross-sectional area during the VDE disruption shown in Fig. 1b. The vertical displacement (Z centroid) grows exponentially, in contrast to the linear behavior exhibited by non-VDE disruptions.
- Figure 5a — Diagram of upper and lower full halo Rogowski coils. The arrows show the flow of halo current into and out of the vessel surface, and through the Rogowski coils.
- 5b — Diagram of toroidal array of 10 halo Rogowski segments
- 5c — Diagram of vertical array of 4 halo Rogowski segments
- Figure 6 — Peak halo current at the top and bottom of the vessel vs I_p for downward disruptions, at fixed toroidal field. Note that the halo current reverses direction when the plasma current is reversed. The solid curve is proportional to $I_p^2 \times \text{sign}(I_p)$. (The value of I_p is taken just prior to the disruption.)

- Figure 7 — Peak halo current at the bottom of the vessel for downward disruptions vs I_p , for all B_ϕ , indicating an inverse scaling with toroidal field. Scalings of the form: I_p^2/B_ϕ or I_p/q_{95} fit the data equally well. (The value of q_{95} is taken just prior to the disruption.)
- Figure 8 — Distribution of the ratio (peak halo current/ I_p) at fixed field and plasma current.
- Figure 9 — Peak instantaneous current quench rate, dI_p/dt , vs I_p . Quench rates up to 1.4 MA/ms have occurred so far.
- Figure 10 — Measurements of the toroidal distribution of halo current from the array of ten divertor shunts at three different times, separated by about 100 μ s. This data is from the non-VDE disruption shown in figure 1a. The arrows show the direction of toroidal motion, which is opposite that of I_p .
- Figure 11 — Measurements of the toroidal distribution of halo current from the array of ten segmented Rogowski coils for the same shot as in the previous figure. The asymmetric pattern and its rotation are the same as that measured by the shunts.
- Figure 12 — Comparison of toroidal distribution of halo currents measured with both the divertor shunts and the segmented Rogowskis. The data is from a disruption that exhibited two complete rotations of the halo current pattern. The two sets of measurements, from two different locations, show the same structure and phase.
- Figure 13 — Data from the vertical array of 4 halo Rogowski segments on the inboard wall for a downward disruption. Only the lowest sensor has appreciable signal.
- Figure 14 — Magnetic flux reconstructions at 1 ms intervals for a midplane-centered disruption. The arrows show *the poloidal projection* of halo current flow, which exists primarily during the last two frames.
- Figure 15 — Data from the vertical array of 4 halo Rogowski segments on the inboard wall for the midplane-centered disruption shown in the previous figure. Halo current is observed on the midplane sensor.

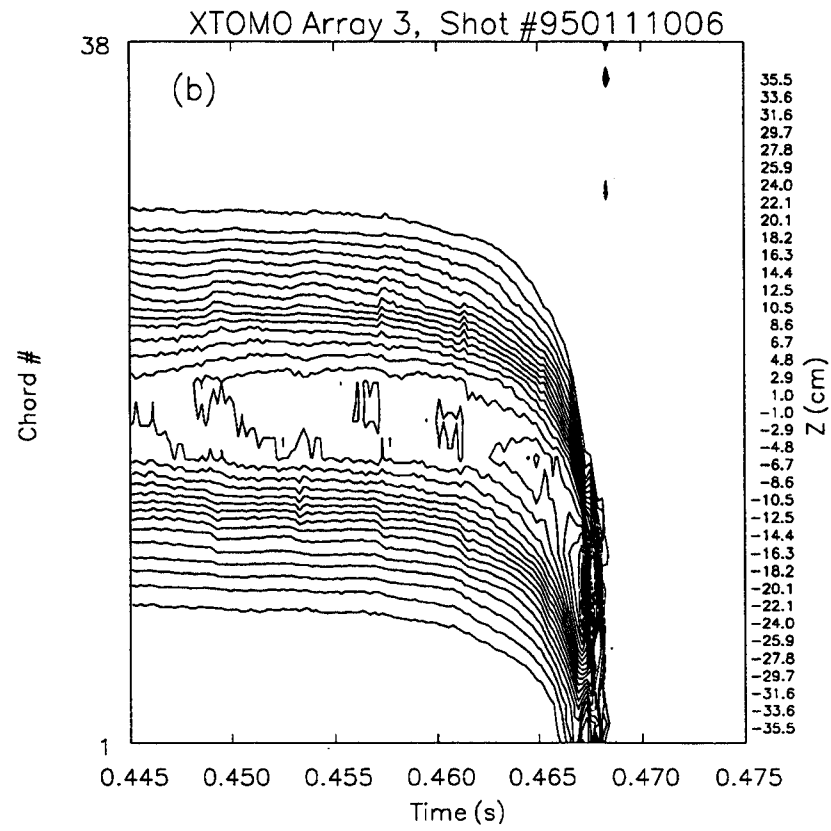
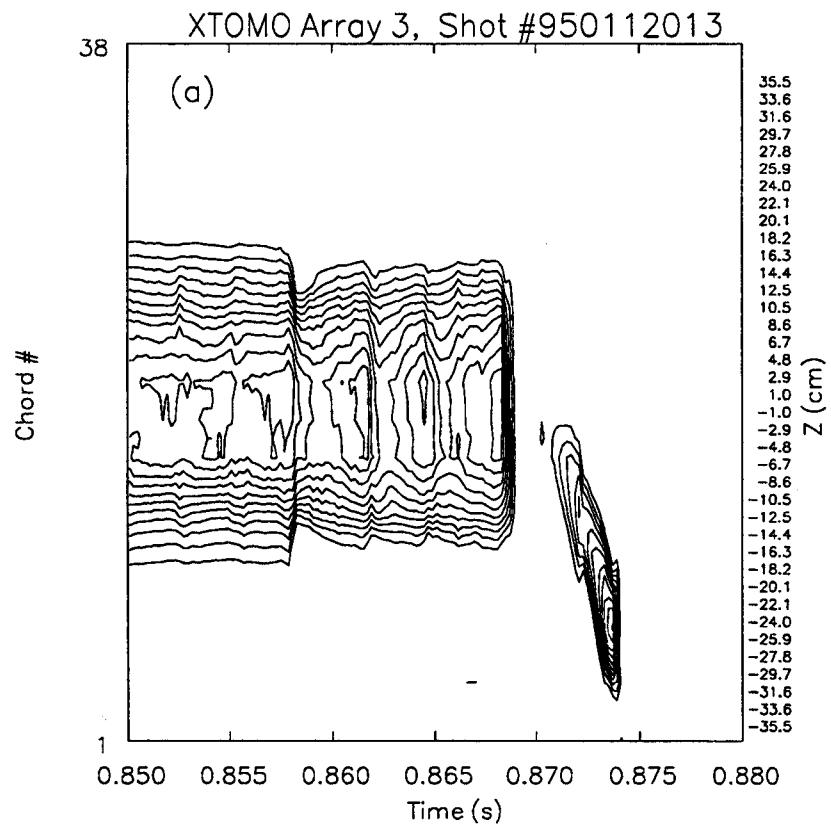


Figure 1

Shot 950112013

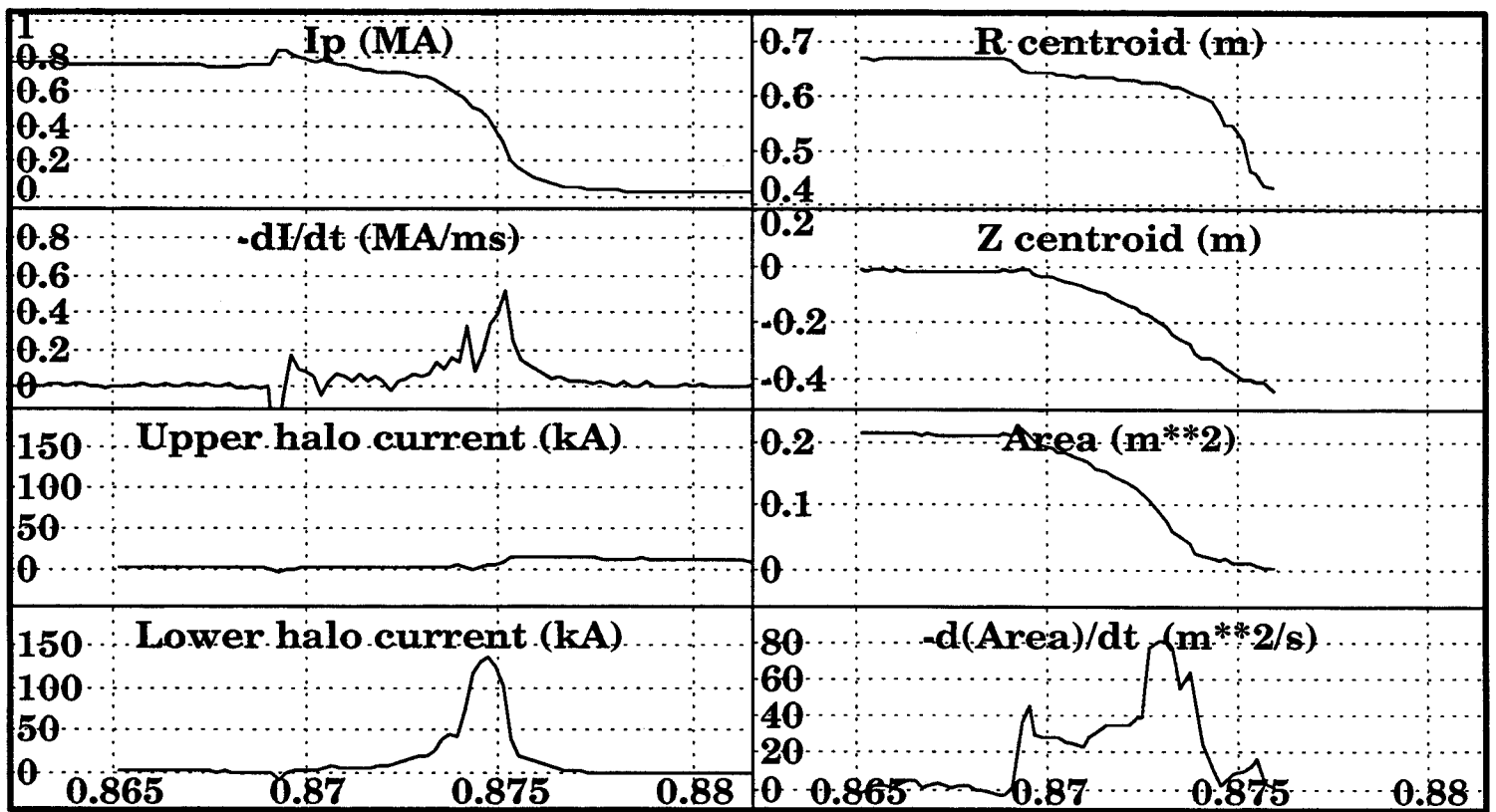


Figure 2

Disruption sequence, shot 950112013

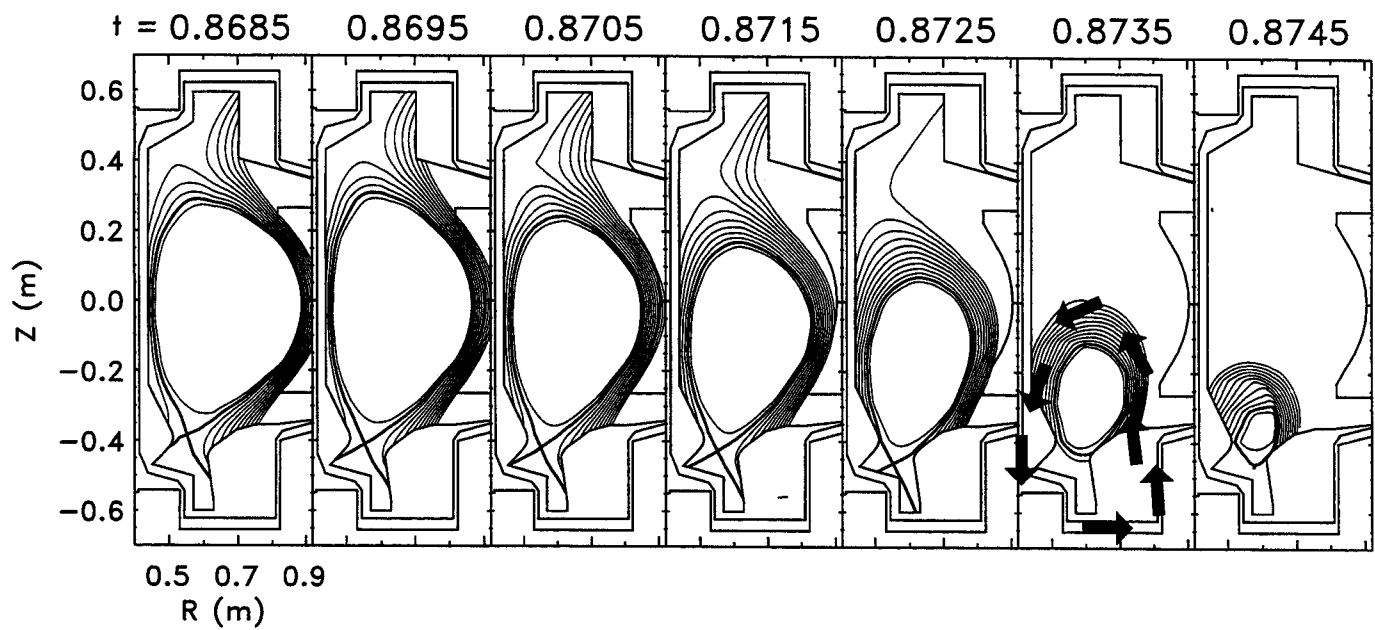


Figure 3

Shot 950111006

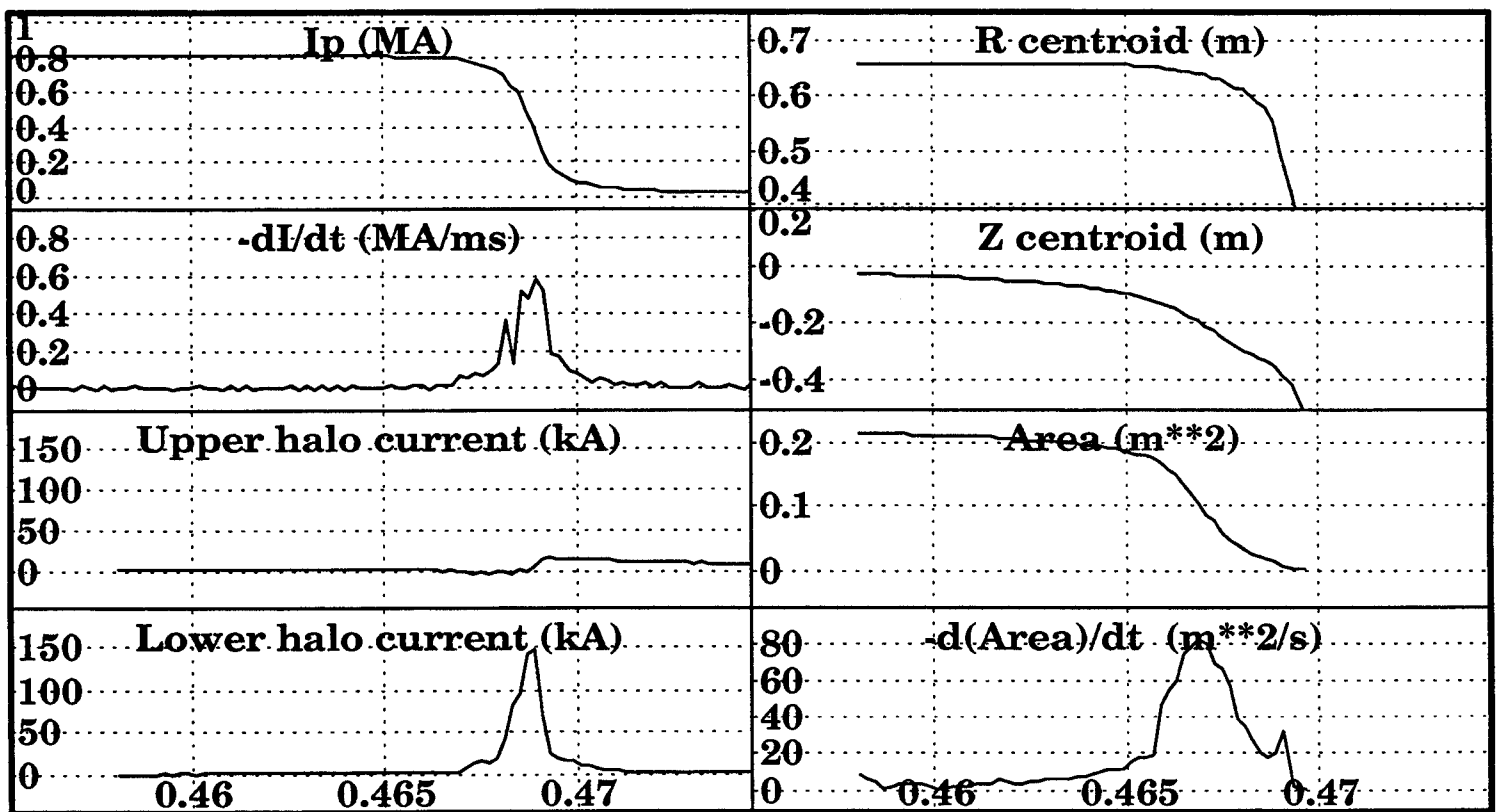


Figure 4

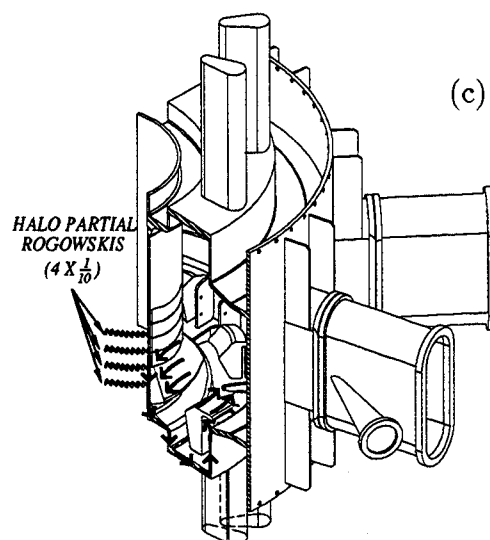
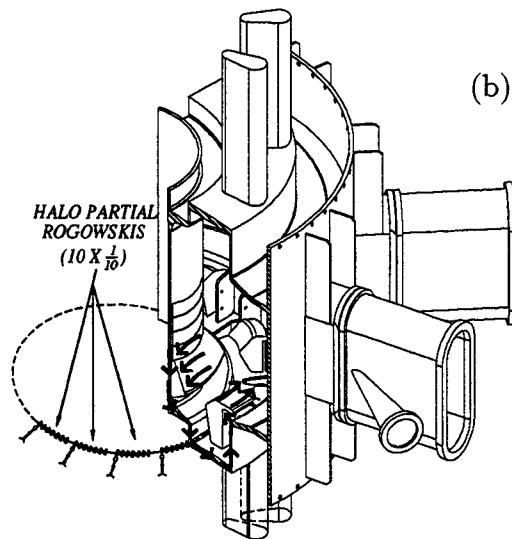
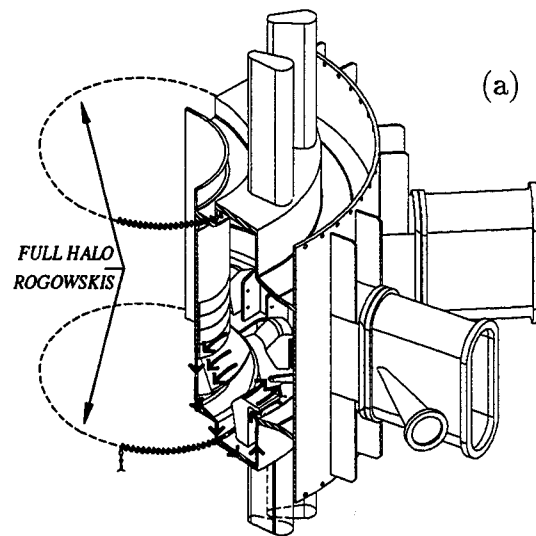


Figure 5

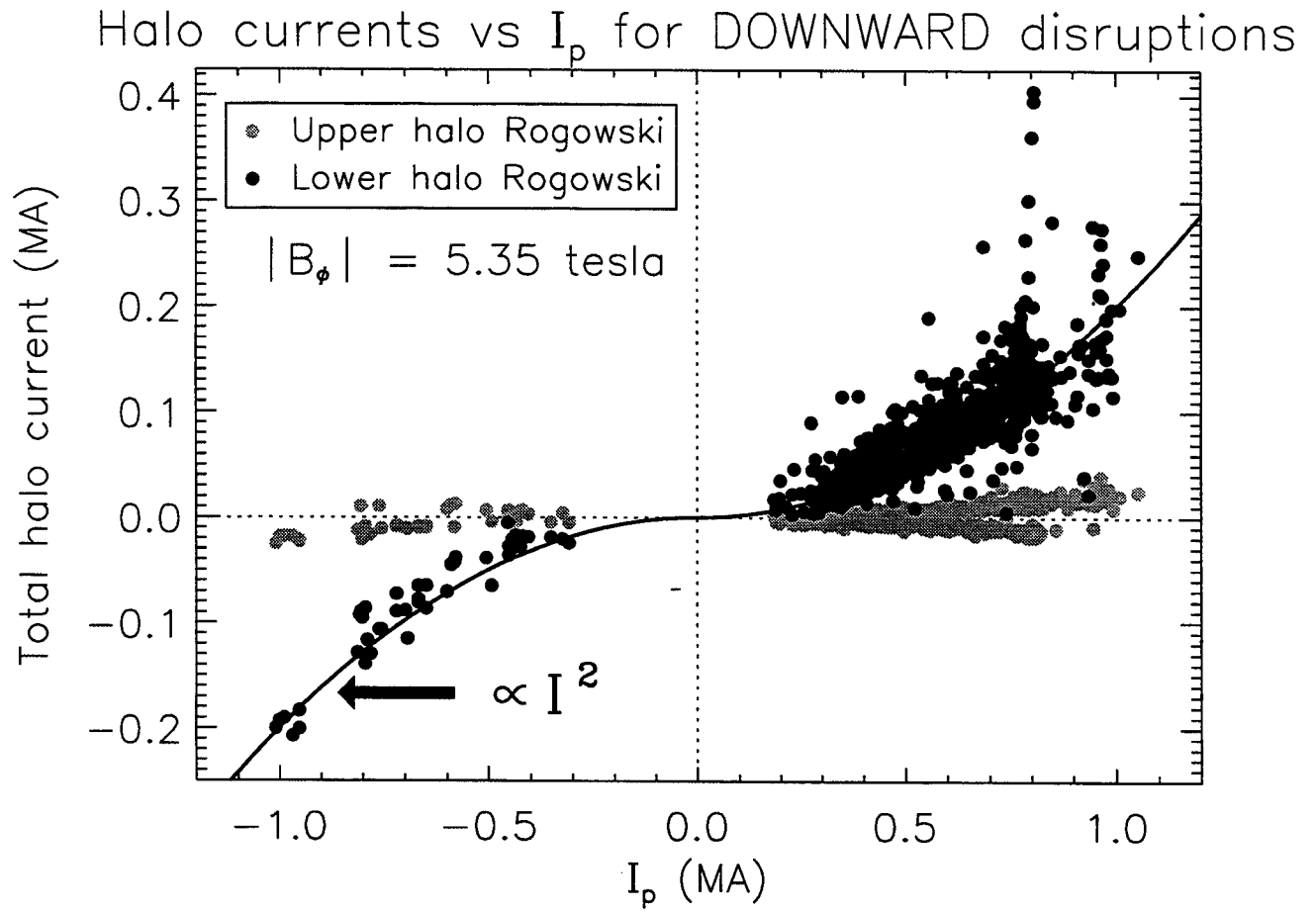


Figure 6

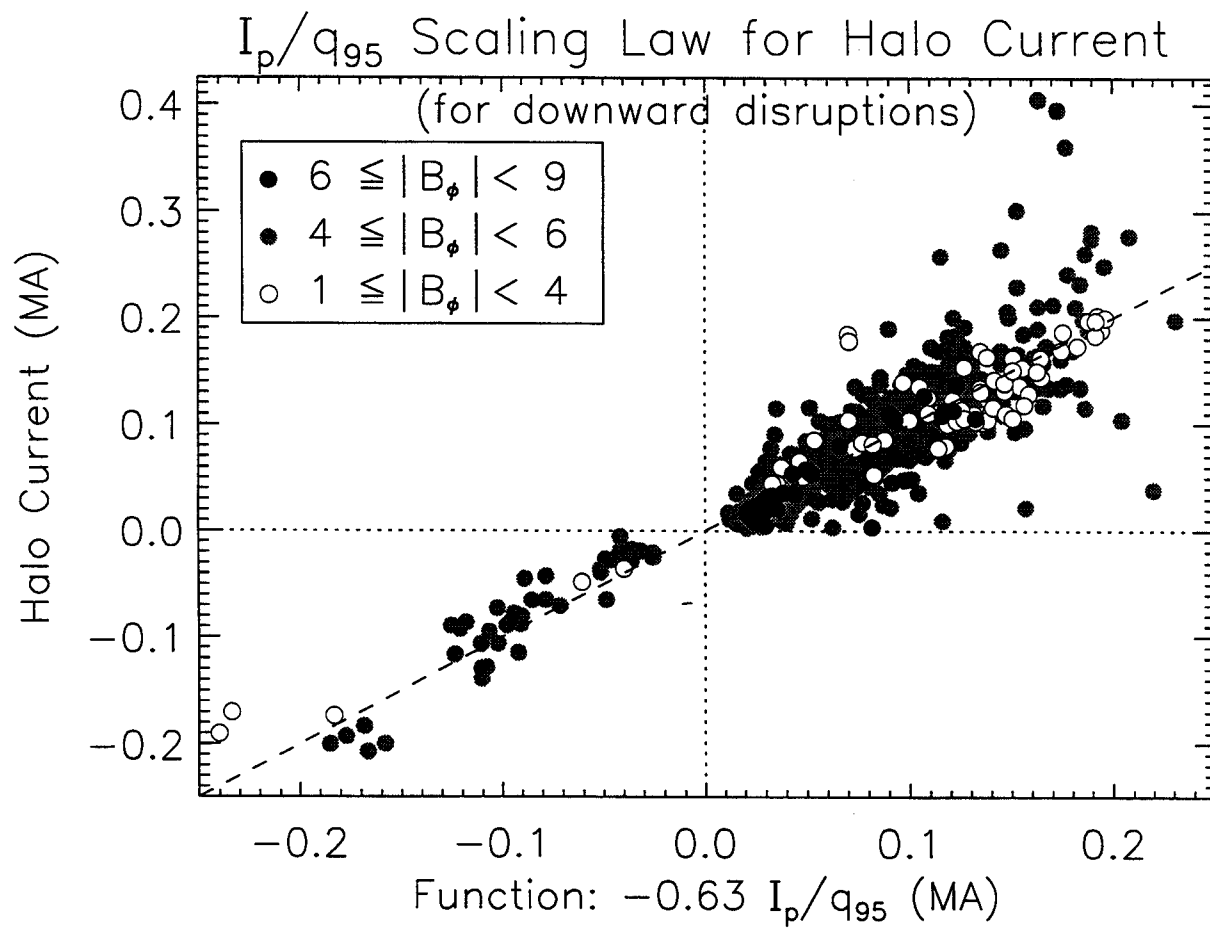


Figure 7

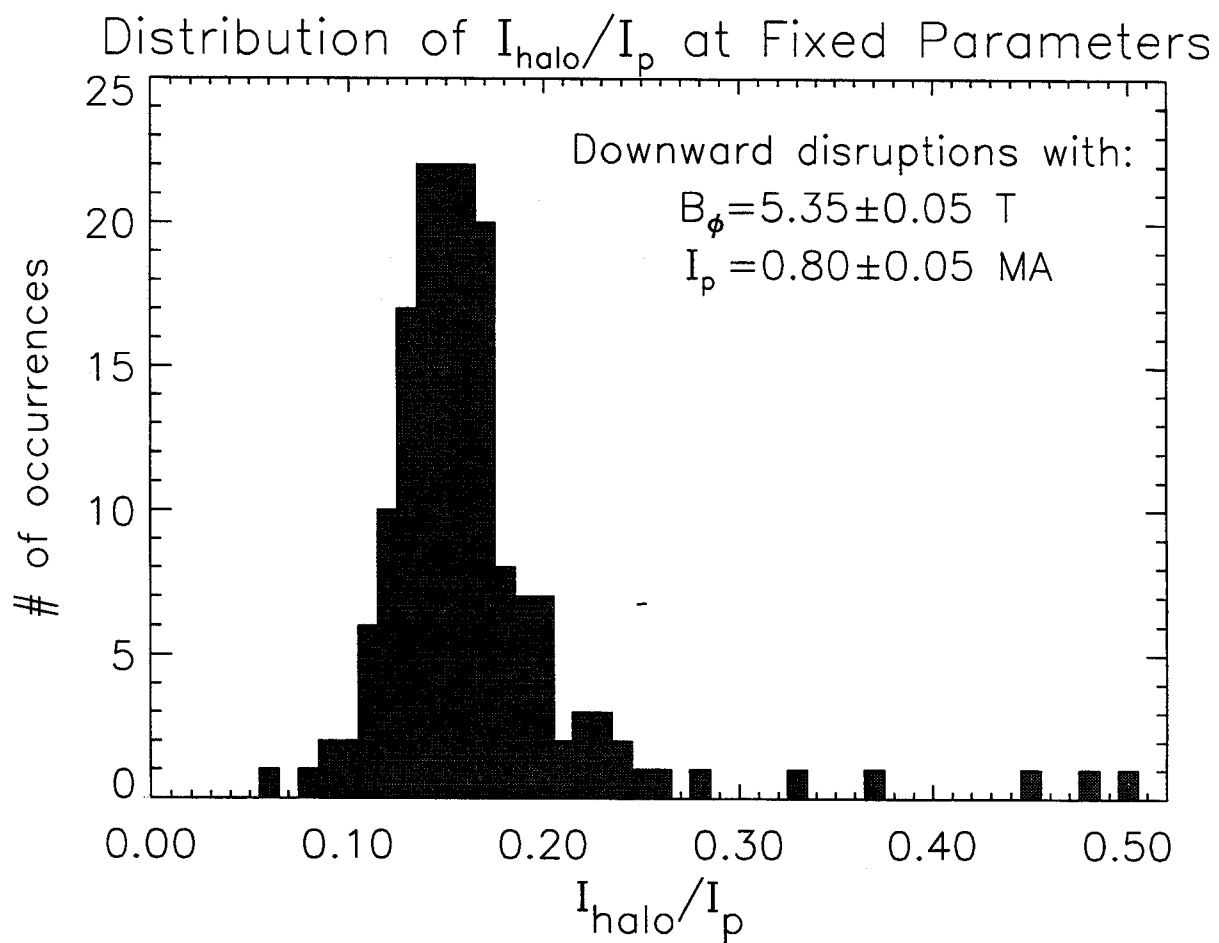


Figure 8

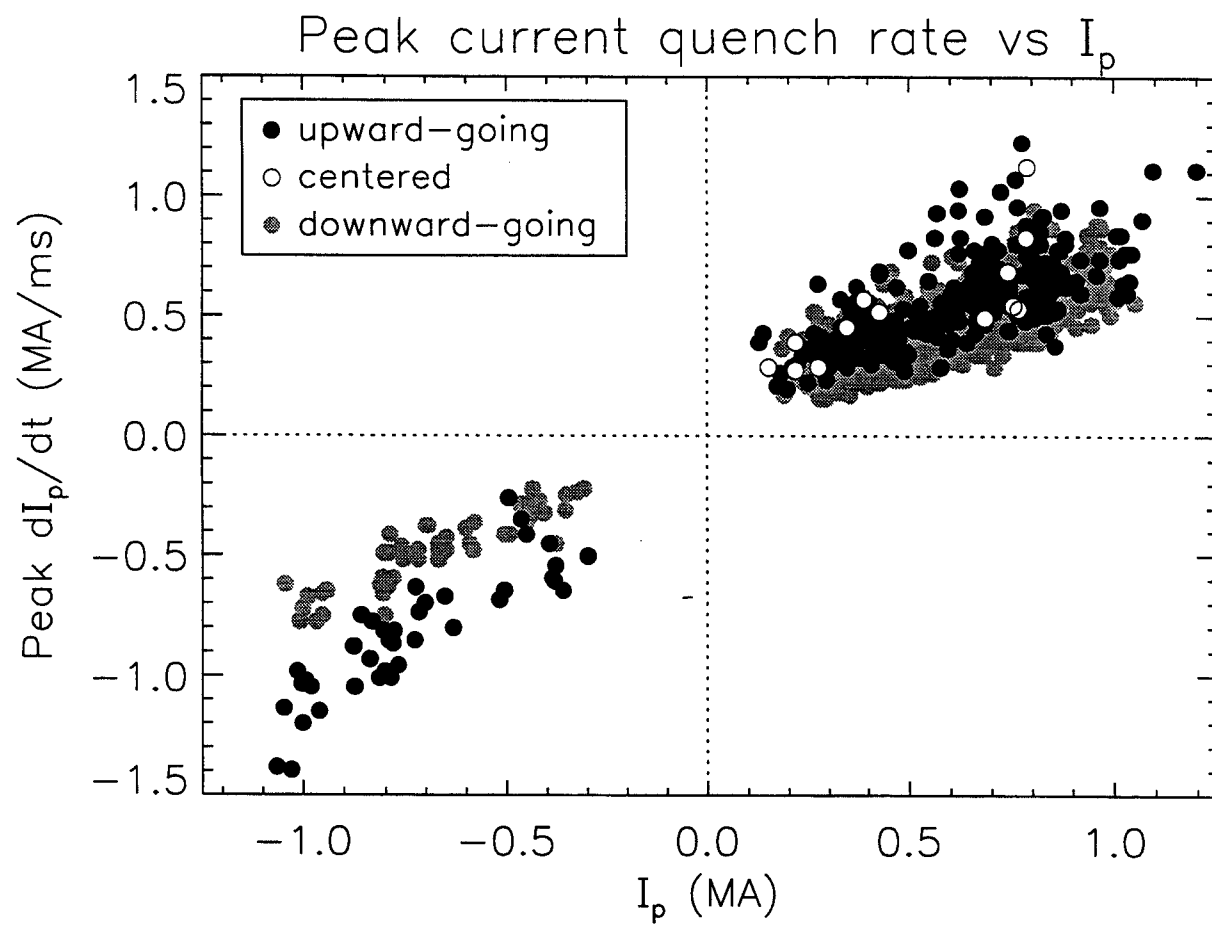


Figure 9

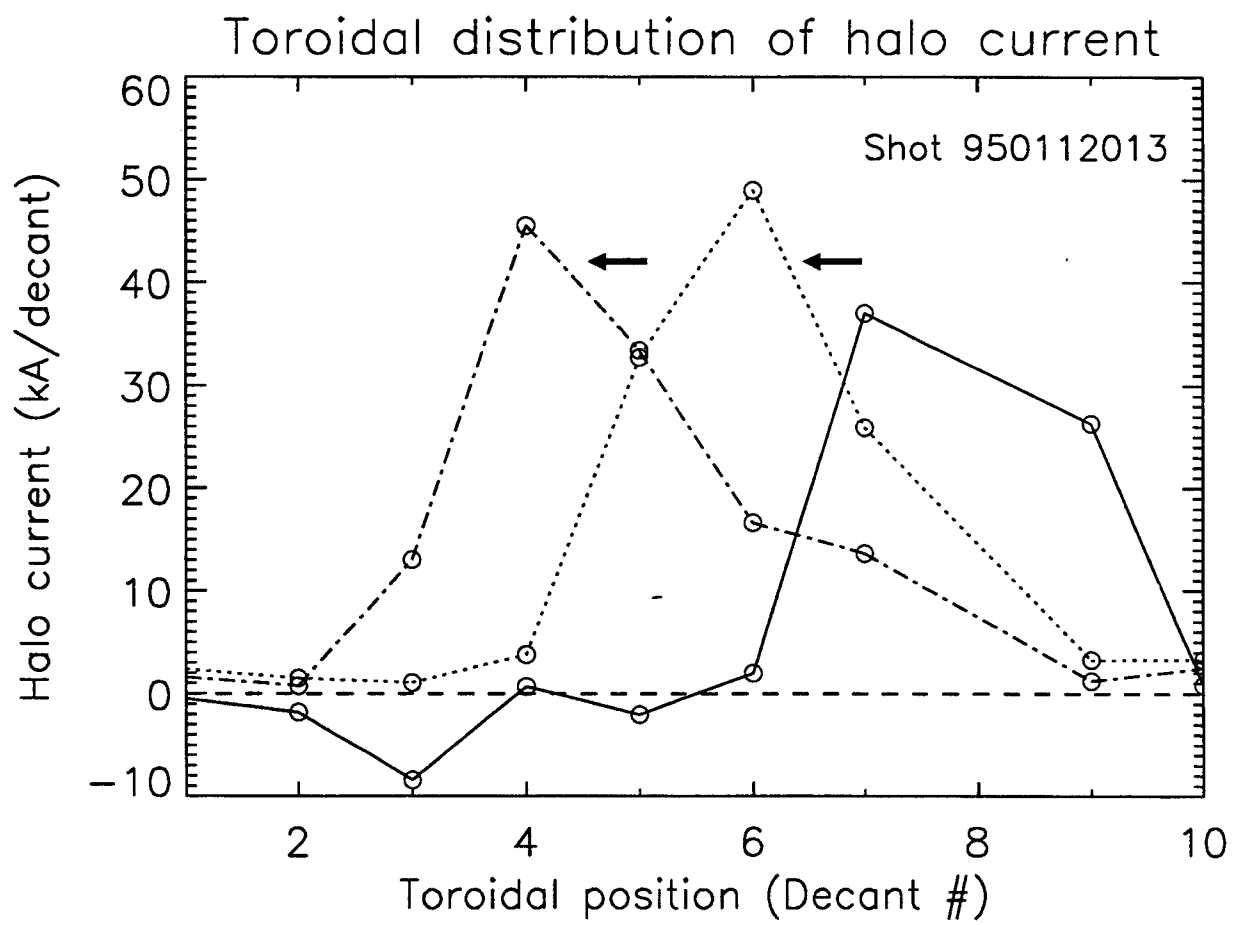


Figure 10

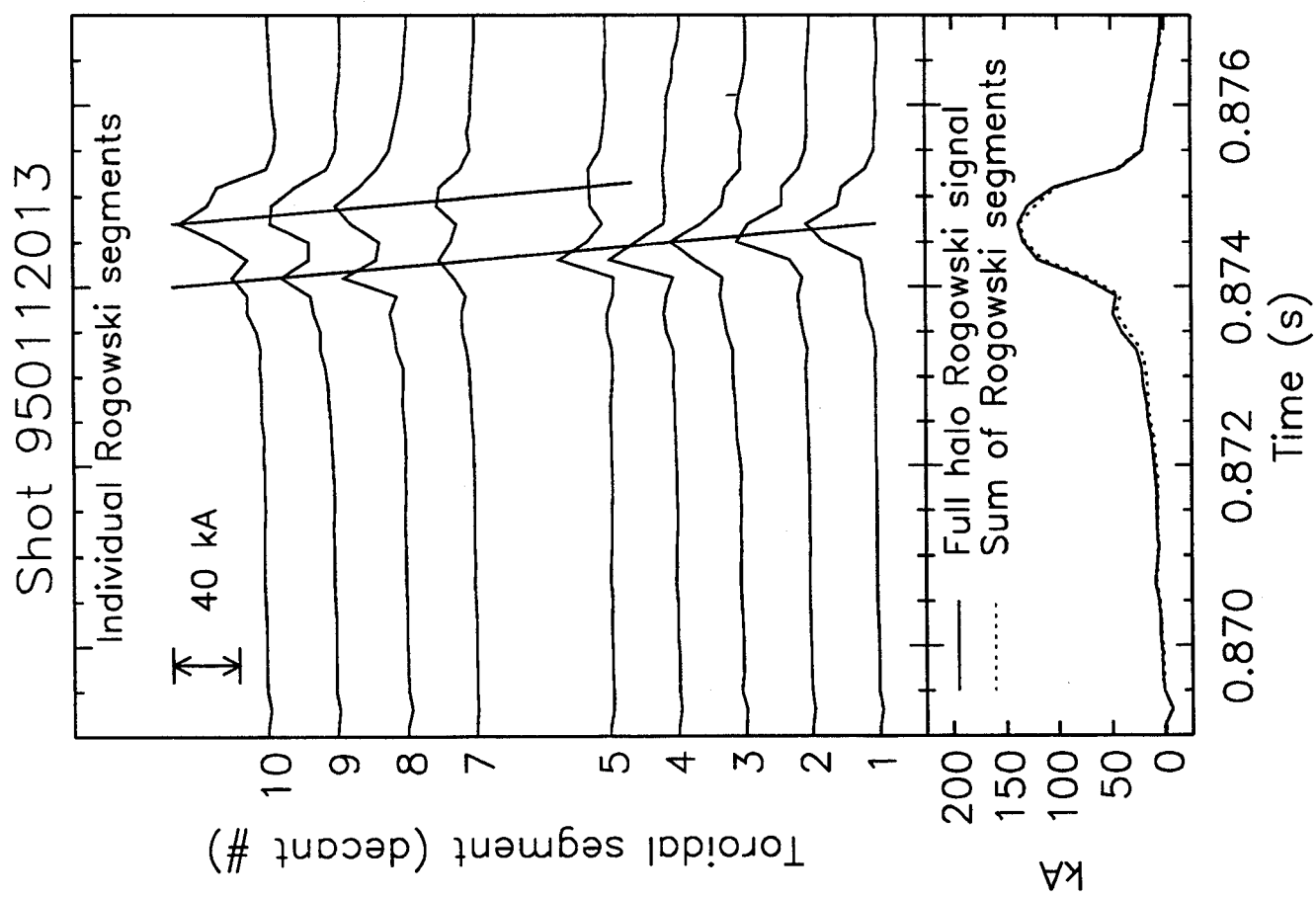


Figure 11

Shot 950120010

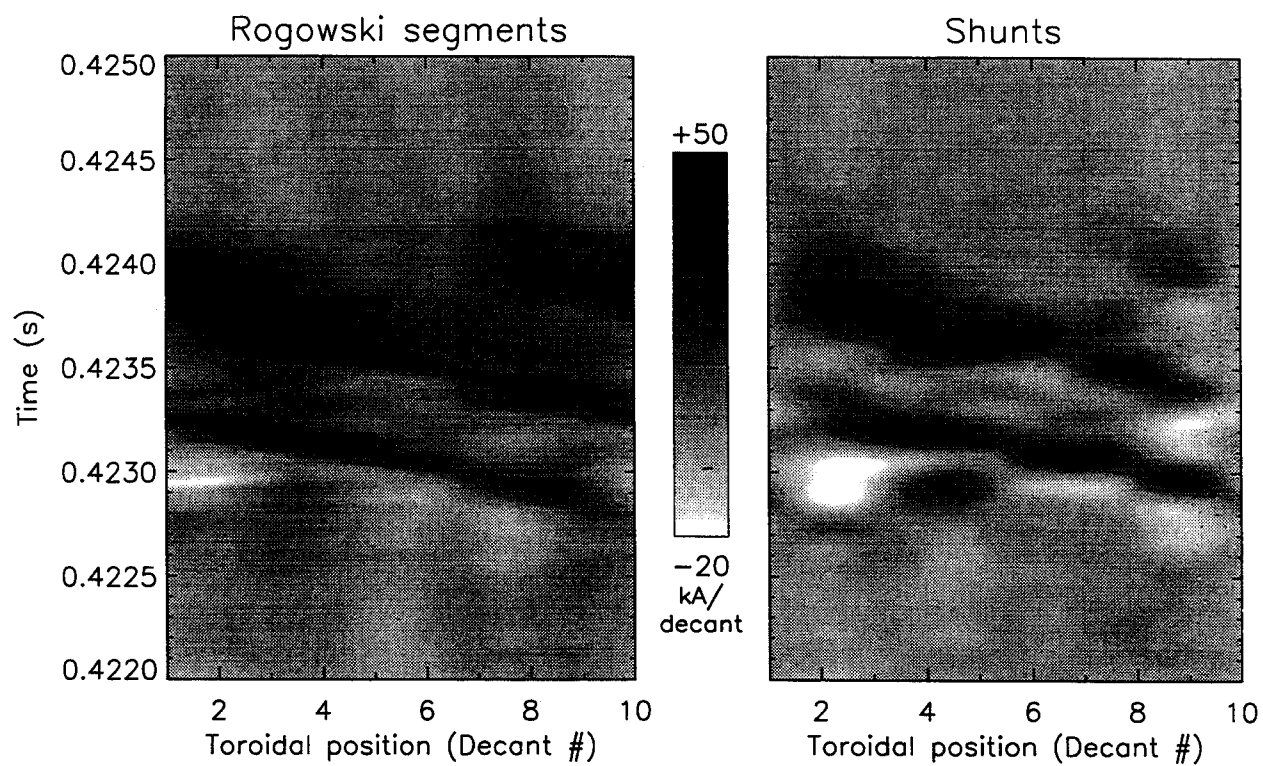


Figure 12

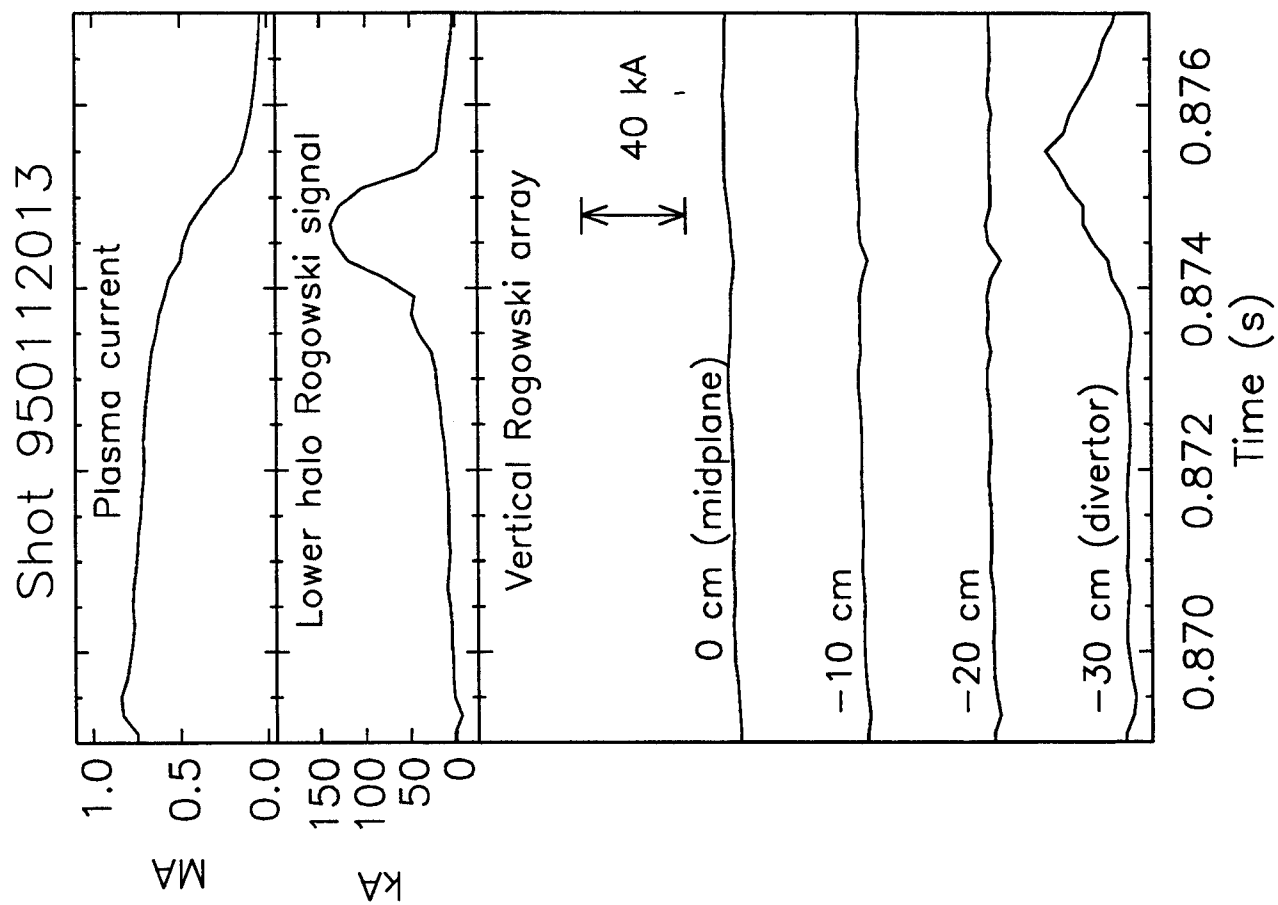


Figure 13

Disruption sequence, shot 950112008

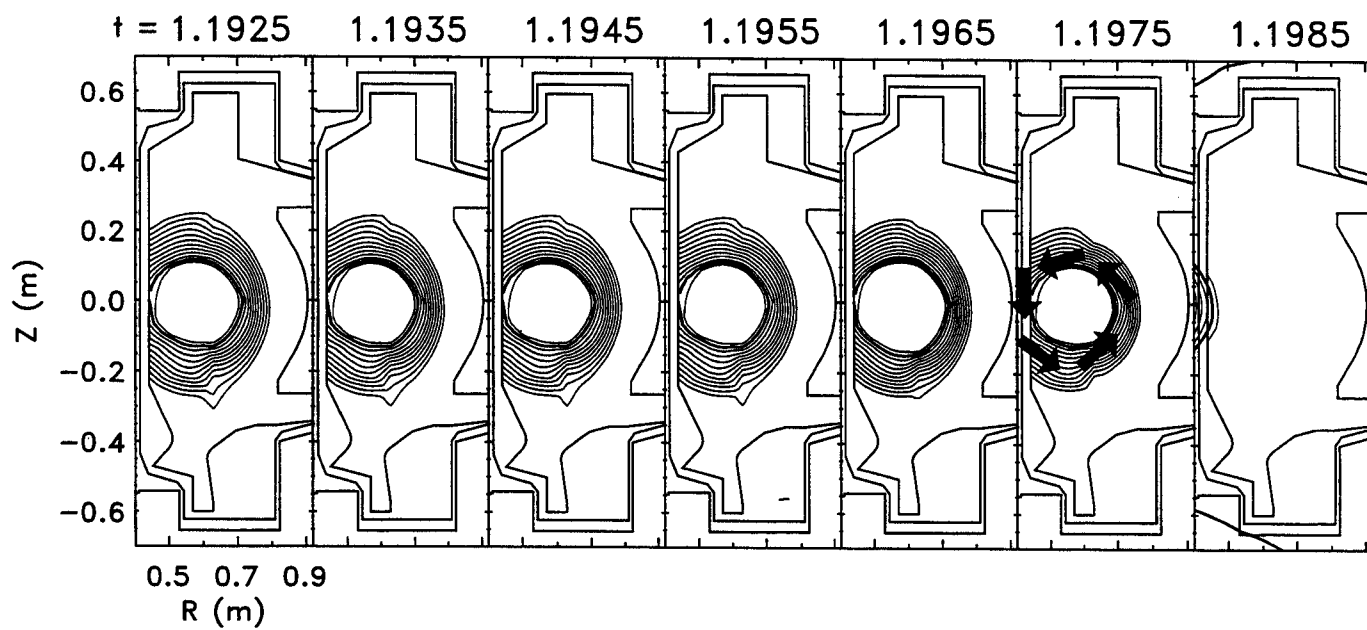


Figure 14

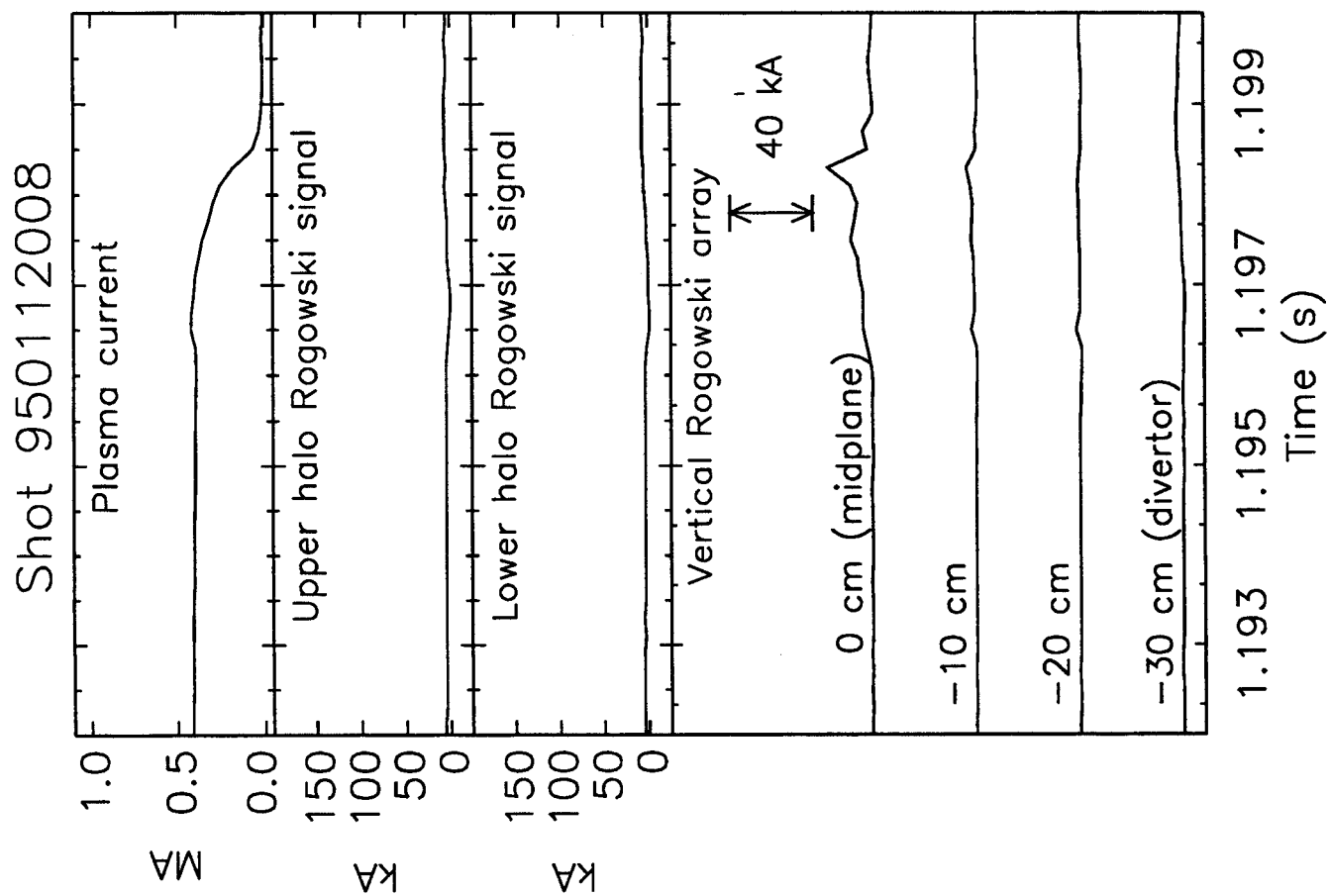


Figure 15